

# Input-specific control of reward and aversion in the ventral tegmental area

Stephan Lammel<sup>1\*</sup>, Byung Kook Lim<sup>1\*</sup>, Chen Ran<sup>1</sup>, Kee Wui Huang<sup>1</sup>, Michael J. Betley<sup>1</sup>, Kay M. Tye<sup>2</sup>, Karl Deisseroth<sup>3</sup> & Robert C. Malenka<sup>1</sup>

**Ventral tegmental area (VTA) dopamine neurons have important roles in adaptive and pathological brain functions related to reward and motivation. However, it is unknown whether subpopulations of VTA dopamine neurons participate in distinct circuits that encode different motivational signatures, and whether inputs to the VTA differentially modulate such circuits. Here we show that, because of differences in synaptic connectivity, activation of inputs to the VTA from the laterodorsal tegmentum and the lateral habenula elicit reward and aversion in mice, respectively. Laterodorsal tegmentum neurons preferentially synapse on dopamine neurons projecting to the nucleus accumbens lateral shell, whereas lateral habenula neurons synapse primarily on dopamine neurons projecting to the medial prefrontal cortex as well as on GABAergic ( $\gamma$ -aminobutyric-acid-containing) neurons in the rostromedial tegmental nucleus. These results establish that distinct VTA circuits generate reward and aversion, and thereby provide a new framework for understanding the circuit basis of adaptive and pathological motivated behaviours.**

The functional roles of VTA dopamine neurons have received great attention because they are the primary source of dopamine in target structures such as the medial prefrontal cortex (mPFC) and nucleus accumbens (NAc), which have important roles in a broad range of motivated behaviours and neuropsychiatric disorders<sup>1–3</sup>. Although dopamine neuron activity often correlates with a reward prediction error (that is, the difference between expected and actual rewards), these cells can also signal aversion, saliency, uncertainty and novelty<sup>2,3</sup>. They are heterogeneous in their anatomical location, targets to which they project, electrophysiological properties and several molecular features<sup>2,4–6</sup>. In addition, the VTA receives both excitatory and inhibitory input from distributed brain areas<sup>2,7,8</sup>. Thus different subpopulations of VTA dopamine and GABAergic neurons may subserve different functions<sup>1,2,4–7,9–15</sup>, but little is known about the afferent control of their activity and the circuits in which they are embedded.

Here we study the function and synaptic connectivity of two main inputs to the VTA from the laterodorsal tegmentum (LDT) and the lateral habenula (LHb). By achieving optogenetic control of LDT and LHb neurons/axons that project directly to the VTA and combining *in vivo* viral-mediated and anatomical-tracing methods with *ex vivo* electrophysiology during stimulation of specific VTA inputs, we define critical differences in the neural circuits responsible for this optogenetic control of reward and aversion.

## Inputs to the VTA from the LDT and LHb

To identify unambiguously the afferent inputs to the VTA, we used a rabies virus in which the glycoprotein is replaced by enhanced green fluorescent protein (RV-eGFP)<sup>16</sup>. Consistent with recent results<sup>17</sup>, injection of RV-eGFP into the VTA resulted in the expression of eGFP in diverse brain areas, with large clusters of eGFP-expressing cells in the PFC, NAc, lateral hypothalamus, LHb and LDT (Supplementary Fig. 1). We focused on inputs to the VTA from the LDT and LHb because both have roles in motivated behaviours by influencing VTA neuronal

activity and the consequent release of dopamine in target structures<sup>2,7,18</sup>. eGFP-positive LDT neurons expressed markers for both glutamatergic neurons (the glutamate transporter EAAC1 (also known as SLC1A1)) and cholinergic neurons (choline acetyltransferase; ChAT) (Supplementary Fig. 2)<sup>19,20</sup>. However, although 95% of LDT neurons projecting to the VTA expressed EAAC1, only ~7% expressed ChAT. LHb neurons are excited by the absence of an expected reward<sup>18</sup> and probably send direct inputs to GABAergic cells in the tail of the VTA, the rostromedial tegmental nucleus (RMTg)<sup>21,22</sup>, that inhibit VTA dopamine neurons<sup>23–26</sup>. eGFP-positive LHb neurons were immunopositive for EAAC1 but not for ChAT (Supplementary Fig. 2), indicating that LHb neurons projecting to the VTA are glutamatergic<sup>8</sup>.

To visualize fibres within the VTA from LDT and LHb we injected the anterograde tracer *Phaseolus vulgaris* leucoagglutinin (PHA-L). It was apparent that the density of LDT and LHb inputs differed between VTA subregions in which different subpopulations of dopamine neurons reside<sup>4,5</sup>. To test this conclusion, we simultaneously retrogradely labelled dopamine projection neurons and anterogradely labelled LDT or LHb fibres (Fig. 1a, h). Injection of PHA-L into the LDT and rabies virus expressing tdTomato (RV-tdTomato) into the NAc lateral shell (Fig. 1a, b) showed that RV-tdTomato cells were predominantly located in the lateral VTA (Fig. 1c), that in close proximity contained LDT terminals as well as tyrosine hydroxylase (TH)-immunopositive processes (Fig. 1d, e). More modest PHA-L labelling was observed in the medial VTA (Fig. 1f) and substantia nigra (Fig. 1g). By contrast, injection of PHA-L into the LHb and RV-tdTomato into the mPFC (Fig. 1h, i) showed RV-tdTomato cells mainly in the medial VTA (Fig. 1j) in close proximity to LHb terminals and TH-immunopositive processes (Fig. 1k, l). There was minimal PHA-L labelling of LHb inputs in the lateral VTA (Fig. 1m) or substantia nigra (Fig. 1n), but as expected<sup>21,22</sup> PHA-L terminals were present in the RMTg adjacent to GABAergic neurons (Supplementary Fig. 3). In additional experiments, we injected fluorescent retrobeads into the NAc lateral shell

<sup>1</sup>Nancy Pritzker Laboratory, Department of Psychiatry and Behavioral Sciences, Stanford University School of Medicine, 265 Campus Drive, Stanford, California 94305, USA. <sup>2</sup>Picower Institute for Learning and Memory, Department of Brain and Cognitive Sciences, Massachusetts Institute of Technology, Cambridge, Massachusetts 02139, USA. <sup>3</sup>Departments of Bioengineering and Psychiatry, Stanford University, Stanford, California 94305, USA.

\*These authors contributed equally to this work.

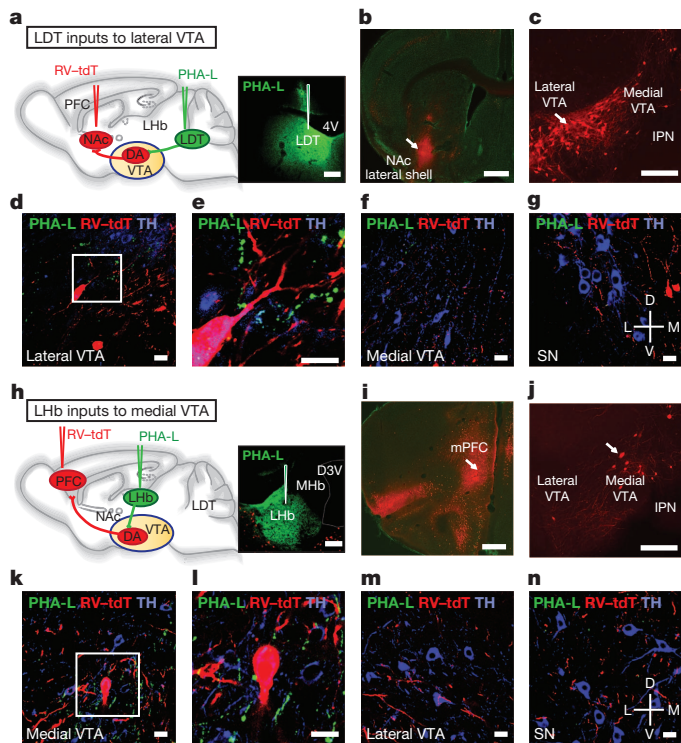


**Figure 1 | LDT and LHB preferentially project to distinct VTA subregions.** **a**, Injection sites for RV-tdTomato (RV-tdT) in the NAc and PHA-L in the LDT. Image shows PHA-L staining in LDT. **b**, RV-tdT in the NAc lateral shell. **c**, VTA neurons projecting to the NAc lateral shell are mainly located in the lateral VTA. **d**, **e**, PHA-L-labelled terminals (green) from the LDT are adjacent to cells projecting to the NAc lateral shell (red) as well as TH-immunopositive processes (blue), with white box in **d** depicting the area shown in **e**. **f**, **g**, Few PHA-L-labelled terminals were detected in the medial VTA (**f**) and in the substantia nigra (SN) (**g**). **h**, Injection sites for RV-tdT in mPFC and PHA-L in LHB. Image shows PHA-L staining in LHB. **i**, RV-tdT in the mPFC. **j**, VTA neurons projecting to the mPFC are mainly located in the medial VTA. **k**, **l**, PHA-L-labelled terminals (green) from the LHB are found adjacent to cells projecting to the mPFC (red) as well as TH-immunopositive processes (blue). White box in **k** depicts area shown in **l**. **m**, **n**, Few PHA-L-labelled terminals were detected in the lateral VTA (**m**) and the substantia nigra (**n**). 4V, fourth ventricle; D3V, dorsal third ventricle; DA, dopamine; IPN, interpeduncular nucleus; MHb, medial habenula. Scale bars, 200  $\mu$ m (**a**–**c**, **h**–**j**), 20  $\mu$ m (**d**–**g**, **k**–**n**).

or mPFC and labelled LDT or LHB inputs with PHA-L, respectively. A similar anatomical distribution of pre- and postsynaptic elements was observed (Supplementary Fig. 3).

### Input-specific control of reward and aversion

These anatomical results suggest that LDT and LHB inputs preferentially terminate in different VTA subregions adjacent to dopamine neuron subpopulations that project to different target structures (NAc lateral shell versus mPFC) and may subserve different behavioural functions<sup>5,6</sup>. To address functional differences in these inputs, we generated a rabies virus expressing the light-activated ion channel channelrhodopsin-2 (ChR2) fused to enhanced yellow fluorescent protein (eYFP; RV-ChR2) (Supplementary Fig. 4) and tested the consequences of the activation of the LDT-VTA and LHB-VTA pathways in a conditioned place preference (CPP) assay by injecting either RV-ChR2 or RV-eGFP into the VTA and implanting an optical fibre over LDT or LHB (Fig. 2a, b). Using a 3-day protocol (Fig. 2c), phasic stimulation of LDT neurons projecting to the VTA on day 2 caused a strong CPP on day 3 (Fig. 2d, f, g), whereas phasic stimulation of LHB neurons projecting to the VTA caused a strong conditioned place aversion (CPA) (Fig. 2e–g). Moreover, after completion of the day-3 testing procedure that involved no optical stimulation (defined as post-test 1),

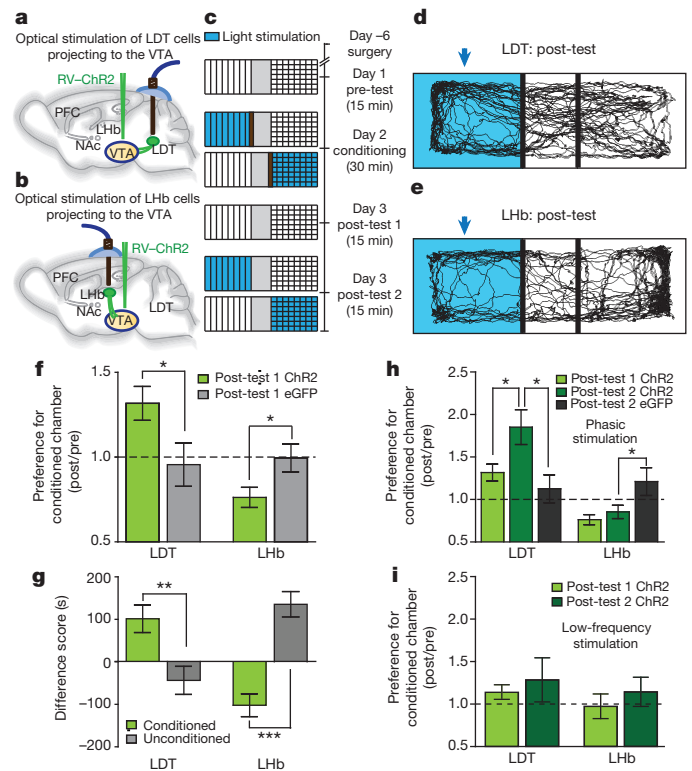


**Figure 2 | Stimulation of LDT and LHB inputs to the VTA elicits CPP and CPA.** **a**, **b**, RV-ChR2 injection into the VTA and optical stimulation of LDT (**a**) and LHB (**b**) projection neurons. **c**, Procedure to elicit and test CPP and CPA. **d**, **e**, Example day-3 mouse tracks, post-test 1. Arrow indicates the chamber in which LDT (**d**) or LHB (**e**) projection neurons were stimulated on day 2. **f**, Post-test 1/pre-test ratio of time spent in conditioned chamber was higher in LDT-ChR2 mice compared to LDT-eGFP mice (LDT-ChR2,  $1.32 \pm 0.1$ ,  $n = 8$ ; LDT-eGFP,  $0.96 \pm 0.13$ ,  $n = 7$ ) but lower in LHB-ChR2 mice (LHB-ChR2,  $0.76 \pm 0.06$ ,  $n = 9$ ; LHB-eGFP,  $0.99 \pm 0.08$ ,  $n = 11$ ). **g**, Differences between post-test 1 and pre-test in time mice spent in conditioned or unconditioned chambers (LDT-ChR2 mice, conditioned chamber,  $105.4 \pm 34.38$ ,  $n = 8$ ; unconditioned chamber,  $-51.1 \pm 26.76$ ,  $n = 8$ ) (LHB-ChR2 mice, conditioned chamber,  $-90.87 \pm 22.59$ ,  $n = 9$ ; unconditioned chamber,  $124.3 \pm 26.27$ ,  $n = 9$ ). **h**, Stimulation of LDT-ChR2 mice during post-test 2 enhanced preference for the conditioned chamber (LDT-ChR2 post-test 1,  $1.32 \pm 0.1$ ,  $n = 8$ ; post-test 2,  $1.85 \pm 0.2$ ,  $n = 8$ ; post-test 2 LDT-eGFP mice,  $1.13 \pm 0.16$ ,  $n = 7$ ). Stimulation of LHB-ChR2 mice during post-test 2 did not cause further aversion (LHB-ChR2 post-test 1,  $0.76 \pm 0.06$ ,  $n = 9$ ; post-test 2,  $0.85 \pm 0.08$ ,  $n = 9$ ), which was still present (LHB-eGFP post-test 2,  $1.22 \pm 0.16$ ,  $n = 11$ ). Post-test 1 results are the same as in **f**. **i**, Low-frequency stimulation of LDT-ChR2 and LHB-ChR2 cells did not elicit CPP or CPA (post-test 1, LDT-ChR2,  $1.13 \pm 0.09$ ,  $n = 6$ ; post-test 2, LDT-ChR2,  $1.28 \pm 0.26$ ,  $n = 6$ ; post-test 1, LHB-ChR2,  $0.97 \pm 0.14$ ,  $n = 7$ ; post-test 2, LHB-ChR2,  $1.14 \pm 0.17$ ,  $n = 6$ ). Error bars denote  $\pm$  s.e.m. \* $P < 0.05$ , \*\* $P < 0.01$ , \*\*\* $P < 0.001$ , Mann-Whitney U-test.

stimulating LDT neurons whenever animals were in the chamber in which they were conditioned on day 2 (defined as day 3, post-test 2) caused a further increase in CPP (Fig. 2h), whereas stimulating LHB neurons did not further enhance CPA (Fig. 2h) (See Supplementary Fig. 5 for non-normalized behavioural results).

Additional results indicate that the effects of stimulating LDT and LHB neurons projecting to the VTA were specific and due to driving activity in distinct populations of VTA neurons. First, animals that received intra-VTA injections of RV-eGFP showed no behavioural effects of phasic optical stimulation in LDT and LHB (Fig. 2f–h and Supplementary Fig. 5). Furthermore, low-frequency stimulation of ChR2 in the LDT and LHB had no effects in the CPP and CPA assays (Fig. 2i and Supplementary Fig. 5). Second, non-stimulated animals showed no preference for either chamber (Supplementary Fig. 4) and

there was no effect of the optogenetic manipulations on time spent in the central chamber (Supplementary Fig. 6). Third, stimulation of LDT and LHB neurons projecting to the VTA had no effects on open-field assays of anxiety or locomotor activity (Supplementary Figs 6 and 7). Fourth, the placement of an optical fibre in the LDT and LHB was confirmed in all animals (Supplementary Fig. 7). Fifth, VTA dopamine neuron activation after LDT and LHB stimulation was quantified by assaying the proportion of TH-immunopositive and TH-immunonegative neurons that expressed the activity-dependent immediate early gene *Fos* (Supplementary Fig. 8). After LDT stimulation, ~40% of dopamine neurons in the lateral VTA expressed FOS, whereas in the medial VTA threefold less dopamine neurons expressed this gene. Activation of LHB inputs to the VTA caused an opposite pattern of FOS expression: ~12% of dopamine neurons in the medial VTA were FOS positive, whereas <2% of dopamine neurons in the lateral VTA expressed FOS. Importantly, ~80% of non-dopamine neurons in the RMTg were FOS positive after LHB stimulation (Supplementary Fig. 8).

On the basis of these results we proposed that LHB inputs drive dopamine neurons in the medial posterior VTA that project to the mPFC<sup>4–6</sup>. To test this prediction, we activated LHB inputs to the VTA in animals in which medial VTA neuron subpopulations that project to different targets were identified by the presence of fluorescent retrobeads (Supplementary Fig. 8). In the medial VTA, ~80% of neurons projecting to the mPFC were FOS positive after LHB stimulation. By contrast, <10% of neurons projecting to the NAc medial shell that are located in the medial VTA<sup>4–6</sup> expressed FOS after LHB stimulation.

Although the FOS results confirm that stimulation of LDT and LHB neurons activated neurons in the VTA, axon collaterals of LDT and LHB neurons may project to other brain regions, activation of which mediated the observed CPP and CPA. To address this possibility, we injected adeno-associated viruses expressing ChR2-eYFP (AAV-ChR2) into the LDT or LHB and stimulated axons of infected neurons using light application directly in the caudal VTA and RMTg (Supplementary Fig. 9). This produced a robust CPP after intra-VTA LDT axonal stimulation and a robust CPA after intra-VTA LHB axonal stimulation (Supplementary Figs 9 and 10). A limitation of these experiments is that intra-VTA activation of LDT and LHB axons may cause antidromic activation of axon collaterals projecting to other brain regions. To address this possibility, we injected RV-eGFP or RV-tdTomato into the VTA and the other virus into brain regions that receive inputs from LDT or LHB<sup>27,28</sup>. If single LDT or LHB neurons projecting to the VTA send collaterals to these other brain regions, the neurons will express both fluorophores. An extremely small number of LDT and LHB neurons projecting to other structures (that is, the ventral pallidum, lateral septum, lateral hypothalamus, mPFC, medio-dorsal thalamic nucleus and supraoculomotor central grey) expressed both fluorophores (Supplementary Fig. 11), indicating that almost all of these neurons project solely to the VTA/RMTg. As a positive control we injected one rabies virus into the VTA and the other into the ventral pallidum, and found that dorsal raphe neurons (~20%), which are known to project to these two structures<sup>29</sup>, expressed both eGFP and tdTomato (Supplementary Fig. 11). We also injected rabies viruses into the VTA and either the LDT or LHB and examined labelling of cells in the other structure. Our results confirm that LDT and LHB have reciprocal anatomical connections<sup>28</sup> but the cells providing these projections do not project to the VTA (Supplementary Fig. 11).

### Synaptic connectivity of LDT and LHB inputs

The results thus far indicate that LDT and LHB inputs activate distinct populations of VTA and RMTg neurons and that this leads to reward and aversion, respectively. To address the specific synaptic connectivity of these inputs, we injected AAV-ChR2 into the LDT and fluorescent retrobeads into target structures of VTA dopamine neurons (Fig. 3a and Supplementary Fig. 12). 8–12 weeks after these injections,

ChR2-eYFP was expressed adjacent to VTA dopamine neurons projecting to the NAc lateral shell (Fig. 3b) and its levels were significantly higher in the lateral VTA (Supplementary Fig. 13). To determine the dopamine neuron populations on which LDT inputs directly synapse, we made whole-cell recordings from retrogradely labelled dopamine neurons projecting to the NAc lateral and NAc medial shell as well as non-labelled dopamine substantia nigra neurons (Fig. 3c, d, f). On average, optical stimulation of LDT fibres generated larger excitatory postsynaptic currents (EPSCs) in dopamine neurons projecting to the NAc lateral shell than in dopamine neurons projecting to the medial shell or dopamine neurons in the substantia nigra (Fig. 3g), all recorded in the same sets of slices. The EPSCs in dopamine neurons projecting to the NAc lateral shell were blocked by an AMPA ( $\alpha$ -amino-3-hydroxy-5-methyl-4-isoxazole propionic acid) receptor antagonist (CNQX, 10  $\mu$ M; Fig. 3c), indicating that LDT fibres released glutamate. Importantly, stimulation of LDT inputs generated EPSCs (>10 pA) in 100% of dopamine neurons projecting to the NAc lateral shell but only in ~30–40% projecting to the NAc medial shell or in the substantia nigra (Fig. 3h). Furthermore, only ~10% of dopamine neurons projecting to the mPFC yielded EPSCs (Fig. 3e, g, h).

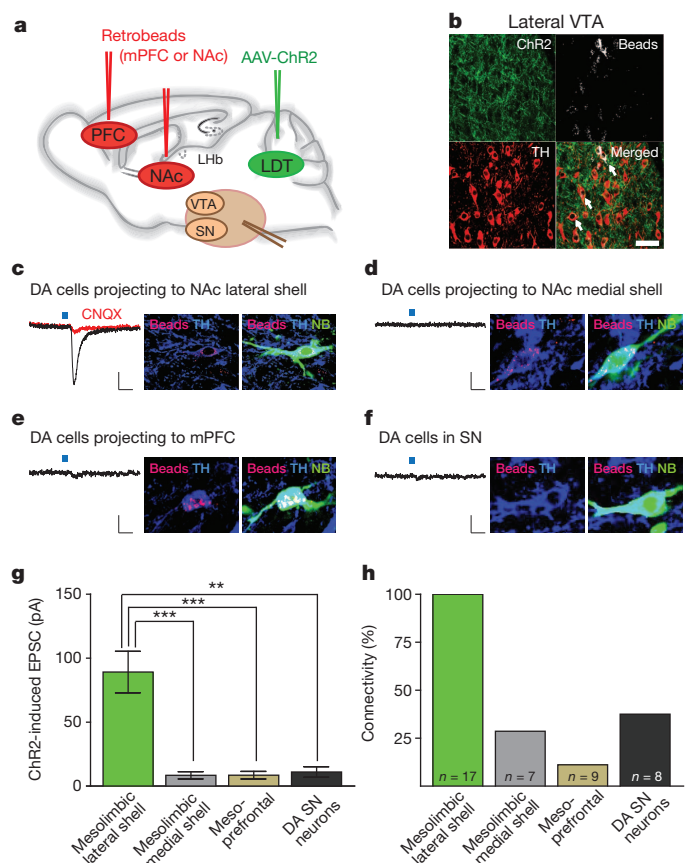


**Figure 3 | LDT neurons preferentially synapse on dopamine neurons projecting to the NAc lateral shell.** **a**, AAV-ChR2 was injected into the LDT and retrobeads were injected into the NAc lateral shell and medial shell, or in the mPFC. **b**, ChR2 expression was in close proximity to retrogradely labelled (beads) TH-immunopositive neurons in the lateral VTA. Scale bar, 50  $\mu$ m. **c–f**, Traces from whole-cell recordings at  $-70$  mV showing EPSCs generated by the stimulation of LDT inputs in retrogradely labelled VTA neurons (beads) projecting to the NAc lateral shell (**c**), NAc medial shell (**d**), mPFC (**e**) or substantia nigra (**f**) neurons. All cells were filled with neurobiotin (NB, green) and are TH-immunopositive (blue). Scale bars, 20 pA 20 ms<sup>-1</sup>. **g**, Summary of average EPSCs generated by optical stimulation of LDT inputs in the four cell populations  $**P < 0.01$ ,  $***P < 0.001$ , one-way analysis of variance (ANOVA) with Bonferroni post-hoc test. Error bars denote  $\pm$  s.e.m. **h**, Percentage of cells in which optical stimulation generated EPSCs >10 pA. *n* values shown in each bar are also applicable to **g**.



The same methodology (Fig. 4a and Supplementary Fig. 12) showed that LHB inputs synapse on a different subpopulation of VTA dopamine neurons as well as on GABAergic cells in the RMTg. ChR2-eYFP-expressing fibres from the LHB were found in the medial posterior VTA in close proximity to dopamine neurons projecting to the mPFC as well as in the RMTg (Supplementary Figs 12 and 13). Importantly, light-evoked EPSCs were generated in 100% of dopamine neurons projecting to the mPFC as well as GABAergic RMTg neurons, whereas detectable EPSCs were not generated in dopamine neurons projecting to the NAc medial shell or lateral shell, nor in substantia nigra neurons (Fig. 4b–g). As LHB inputs preferentially synapse on dopamine neurons projecting to the mPFC and RMTg GABAergic cells, we predicted that LHB inputs may inhibit dopamine neurons projecting to the NAc lateral shell through feed-forward inhibition. Indeed, in ~60% of dopamine neurons projecting to the NAc lateral shell, stimulation of LHB inputs evoked inhibitory postsynaptic currents (IPSCs; Fig. 4h, i). By contrast, stimulation of LHB axons did not generate detectable IPSCs in dopamine neurons projecting to the NAc medial shell (Fig. 4h).

These results suggest that LDT and LHB inputs to VTA preferentially activate distinct populations of dopamine neurons that project to different target structures and that, in addition, LHB inputs activate GABAergic cells in the RMTg and perhaps within the VTA itself. Such differences in connectivity can explain the different behavioural consequences of LDT and LHB stimulation (Fig. 2). To further test these conclusions, we generated AAVs expressing a double-floxed rabies virus glycoprotein (AAV-double-floxed inverted open-reading frame (DIO)-RVG) and infected the VTA in TH-Cre mice so that the glycoprotein was only expressed in dopamine neurons (Fig. 5a). Two weeks later, RV-eGFP and RV-tdTomato were injected into the mPFC and NAc lateral shell, respectively (Fig. 5a, b). Because RV-eGFP and RV-tdTomato lack the RVG, expression of eGFP and tdTomato is restricted to initially infected cells<sup>16</sup>. However, in VTA dopamine neurons projecting to these targets (Fig. 5c), transcomplementation with

RVGs occurs and allows RV-eGFP and RV-tdTomato to spread retrogradely, thus labelling cells that synaptically contact the dopamine neurons. After rabies virus injections, cells in the LDT were clearly labelled with tdTomato with almost no cells expressing eGFP (tdTomato,  $n = 18.75 \pm 7.12$  cells per animal; eGFP,  $n = 1.25 \pm 0.75$ ;  $n = 4$  mice; Fig. 5d), whereas LHB cells were clearly labelled with eGFP with almost no cells expressing tdTomato (eGFP,  $8.25 \pm 3.44$  cells; tdTomato,  $0.5 \pm 0.22$ ;  $n = 4$  mice; Fig. 5e). When AAV-DIO-RVG was not injected into the VTA before rabies virus injections, no tdTomato-positive or eGFP-positive cells in the LDT or LHB, respectively, were observed ( $n = 3$  mice) (Fig. 5f, g). These results confirm that LDT neurons preferentially synapse on VTA dopamine neurons projecting to the NAc lateral shell and LHB neurons preferentially synapse on VTA dopamine cells projecting to the mPFC.

### D1/D2R antagonists in mPFC and NAc lateral shell

Activation of VTA GABAergic cells alone can elicit CPA<sup>13</sup> and disrupt reward consummatory behaviour<sup>15</sup>. These results raise the question of whether activation of dopamine neurons projecting to the mPFC is necessary for the CPA elicited by activation of LHB inputs to the VTA and RMTg. To address this question, we infused the D1 dopamine receptor antagonist SCH23390 into the mPFC immediately before stimulating LHB neurons projecting to the VTA and RMTg (Fig. 5h). This manipulation, which does not impair cocaine CPP<sup>30</sup>, prevented the occurrence of CPA, which was elicited in control animals that received vehicle injections into the mPFC (Fig. 5i, j and Supplementary Fig. 14). Similarly, infusion of D1 and D2 receptor antagonists into the NAc lateral shell, but not infusion of vehicle, prevented the CPP elicited by activation of LDT neurons projecting to the VTA (Fig. 5k–m and Supplementary Fig. 14). Control experiments showed that infusion of dopamine receptor antagonists alone into either the mPFC or NAc lateral shell did not elicit CPP or CPA compared to animals that received vehicle infusions ( $n = 4$  mice in each group;  $P > 0.05$ , Mann–Whitney U-test). These results provide further evidence that activation

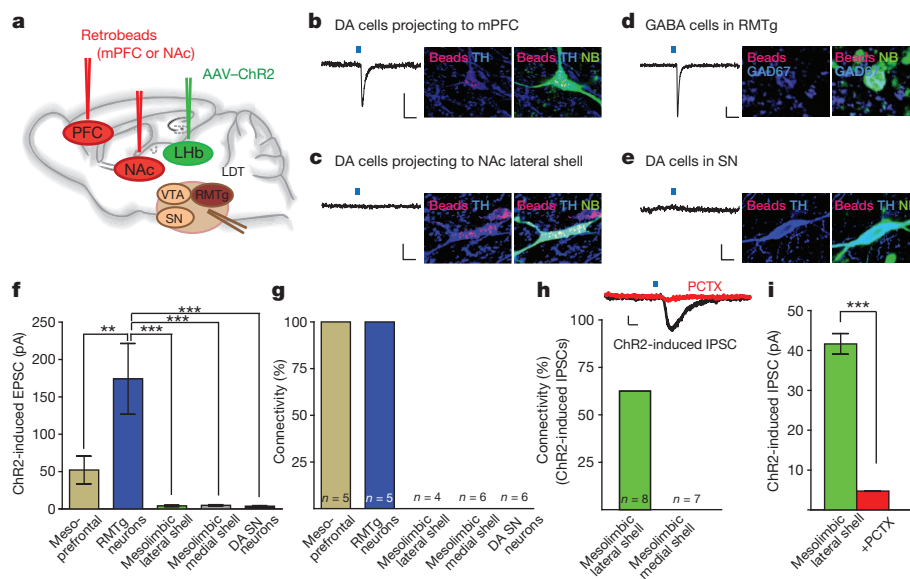


**Figure 4 | LHB neurons preferentially synapse on dopamine neurons projecting to the mPFC and RMTg GABAergic neurons.** **a**, AAV-ChR2 was injected into the LHB and retrobeads were injected into either the NAc lateral shell and medial shell or in the mPFC. **b–e**, Traces from whole-cell recordings at  $-70$  mV showing EPSCs generated by optical stimulation of LHB inputs in retrogradely labelled VTA neurons (beads, red) projecting to the mPFC (**b**), NAc lateral shell (**c**) an RMTg cell (**d**) and substantia nigra cell (**e**). All cells were filled with neurobiotin (green) and are either TH-immunopositive (blue) (**b**, **c**, **e**) or GAD67-immunopositive (blue, **d**). Scale bars, 20 pA 20 ms<sup>-1</sup>. **f**, Summary of average EPSCs generated by optical stimulation of LHB inputs in

five cell populations. \*\* $P < 0.01$ , \*\*\* $P < 0.001$ , one-way ANOVA with Bonferroni post-hoc test. Error bars denote  $\pm$  s.e.m. **g**, Percentage of cells in which optical stimulation generated EPSCs  $>10$  pA.  $n$  values shown in each bar are also applicable to **f**. **h**, Optical stimulation of LHB inputs generates an IPSC in dopamine cells projecting to the NAc lateral shell. Scale bars, 20 pA 20 ms<sup>-1</sup>. Graph shows the percentage of dopamine cells projecting to the NAc lateral shell or medial shell in which IPSCs were generated by LHB input stimulation. **i**, Average IPSC size from dopamine cells projecting to the NAc lateral shell. IPSCs were blocked by picrotoxin.  $n = 3$ ; \*\*\* $P < 0.0001$ , unpaired Student's  $t$ -test. PCTX, picrotoxin.

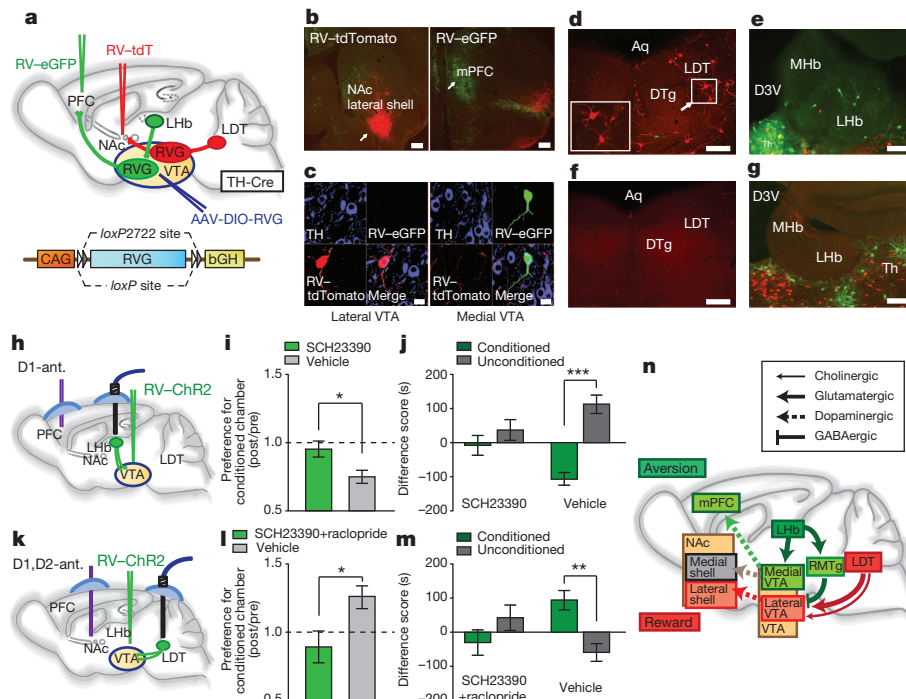


**Figure 5 | Rabies virus reveals distinct VTA circuits and effects of dopamine receptor antagonists on CPP and CPA.** **a**, AAV expressing RVG in a Cre-dependent manner was injected into the VTA of TH-Cre mice. RV-eGFP and RV-tdTomato, injected subsequently into the mPFC and NAc, respectively, were retrogradely transported to subpopulations of dopamine neurons in which transcomplementation occurs, allowing the rabies virus to spread retrogradely and label cells that synaptically contact infected dopamine neurons. **b**, Injection sites in the NAc lateral shell (RV-tdTomato; left) and mPFC (RV-eGFP; right). **c**, TH-immunoreactive neurons in the lateral VTA (left) and medial VTA (right) retrogradely labelled by RV-tdTomato or RV-eGFP. **d**, **e**, tdTomato and eGFP labelling in LDT (**d**) and LHb (**e**) neurons, respectively, when injection of AAV-DIO-RVG into the VTA of TH-Cre mice was performed before rabies virus injections. **f**, **g**, Lack of tdTomato expression in LDT (**f**) and lack of eGFP expression in LHb (**g**) after virus injections in TH-Cre mice that were not injected with AAV-DIO-RVG. **h**, Placements of drug-infusion cannula into the mPFC and optic fibre into the LHb, as well as injection of RV-ChR2 into the VTA. **i**, Ratio of post-test/pre-test time spent in the conditioned chamber when either SCH23390 or vehicle was infused into the mPFC before LHb optical stimulation (SCH23390,  $0.95 \pm 0.05$ ,  $n = 9$ ; vehicle,  $0.75 \pm 0.04$ ,  $n = 7$ ). **j**, Difference between post-test and pre-test in the time mice

spent in the conditioned or unconditioned chambers after LHb stimulation (SCH23390, conditioned chamber,  $-7.24 \pm 28.79$ , unconditioned chamber,  $36.83 \pm 30.74$ ,  $n = 9$ ; vehicle, conditioned chamber,  $-106.88 \pm 18.82$ , unconditioned chamber,  $112.61 \pm 26.48$ ,  $n = 7$ ). **k**, Placements of drug-infusion cannula into the NAc lateral shell and optic fibre into the LDT, as well as injection of RV-ChR2 into the VTA. **l**, Ratio of post-test/pre-test time spent in the conditioned chamber when SCH23390 and raclopride or vehicle were infused into the NAc lateral shell before LDT optical stimulation (SCH23390/raclopride,  $0.89 \pm 0.1$ ,  $n = 7$ ; vehicle,  $1.26 \pm 0.08$ ,  $n = 6$ ). **m**, Difference between post-test and pre-test in time mice spent in conditioned or unconditioned chamber after LDT stimulation (SCH23390/raclopride, conditioned chamber,  $-30.17 \pm 37.38$ , unconditioned chamber,  $42.22 \pm 34.68$ ,  $n = 7$ ; vehicle, conditioned chamber,  $94.58 \pm 27.77$ , unconditioned chamber,  $-59.38 \pm 26.44$ ,  $n = 6$ ).  $*P < 0.05$ ,  $**P < 0.01$ ,  $***P < 0.001$ , Mann-Whitney U-test. Error bars denote  $\pm$  s.e.m. **n**, Proposed circuits driven by LDT and LHb inputs into the VTA. Green shading indicates circuit involved in aversion and red/pink shading indicates circuit involved in reward and salience. ant., antagonist; Aq, aqueduct; DTg, dorsal tegmental nucleus; Th, thalamus. Scale bars, 200  $\mu$ m (**b**), 20  $\mu$ m (**c**), 100  $\mu$ m (**d**–**g**).

of different subpopulations of VTA dopamine neurons and the consequent release of dopamine in different target structures are necessary for mediating the reward and aversion generated by activation of LDT and LHb inputs, respectively.

### Concluding remarks

A fundamental task of the mammalian brain is to assign emotional/motivational valence to environmental stimuli by determining whether they are rewarding and should be approached or are aversive and should be avoided. Internal stimuli also are assigned emotional/motivational valence and prevalent brain disorders, such as addiction and depression, involve pathological dysfunction in the performance of these tasks. Although VTA dopamine neurons have a role in reward-dependent behaviours<sup>1–3,7,10,12,14,31,32</sup> and inhibition of VTA dopamine neurons by GABAergic neurons contributes to reward prediction error calculations and promotes behaviours associated with aversion<sup>10,12,13,15</sup>, the detailed circuits within the VTA that mediate reward and aversion and their control by upstream brain areas have not been defined. By combining virus-mediated tracing, synaptic electrophysiology and *in vitro* and *in vivo* optogenetic manipulations, we have presented evidence that two main inputs to the VTA from the

LDT and LHb trigger reward- and aversion-associated behaviours, respectively, through activation and di-synaptic inhibition of distinct subpopulations of VTA dopamine neurons that project to different target structures. These findings indicate that there are several subpopulations of VTA dopamine neurons embedded in distinct circuits that contribute to different behavioural functions (Fig. 5n). Dopamine neurons projecting to the mPFC may be the primary subpopulation of dopamine neurons that are preferentially activated by aversive stimuli, although these neurons likely subserve other important functions<sup>33</sup>. On the other hand, dopamine neurons projecting to the NAc lateral shell may primarily signal reward and perhaps salience<sup>2,5</sup>. This hypothesis is consistent with studies measuring the release of dopamine in target structures after stimulation of LDT and LHb, as well as recent optogenetic manipulations of VTA dopamine neuron activity<sup>10,19,31,32,34</sup>.

Although LDT and LHb inputs activate different cell populations in the VTA and RMTg, it is probable that these distinct 'circuits' do not routinely function in isolation. They interact with one another anatomically<sup>28</sup> (Supplementary Fig. 11) and functionally (Fig. 4). Indeed, stimuli can have both rewarding and aversive qualities simultaneously and these qualities can change depending on the context.

Thus, LDT and LHB inputs to the VTA and RMTg can be conceptualized as belonging to a more complex global brain system that assigns motivational valence or value to external and internal stimuli. Further elucidation of the detailed synaptic connectivity of LHB inputs to the VTA may be particularly interesting in the context of the potential role of LHB in psychiatric disorders such as depression and schizophrenia<sup>18,35–37</sup>. Overactivity of LHB neurons would be expected to drive depressive symptoms such as anhedonia, whereas LHB pathology in schizophrenia may contribute to the cognitive symptoms that are associated with PFC dysfunction<sup>37</sup>.

**Note added in proof:** A recent paper also finds that optogenetic activation of LHB efferents to the midbrain is aversive<sup>38</sup>.

## METHODS SUMMARY

Male adult (10–12 weeks of age) C57BL/6 (Charles River) or TH-Cre (B6.Cg-Tg(Th-cre)1Tmd/J; Jackson Laboratory) mice were used for all experiments. All procedures complied with the animal care standards set forth by the National Institutes of Health and were approved by Stanford University's Administrative Panel on Laboratory Animal Care.

**Full Methods** and any associated references are available in the online version of the paper.

**Received 23 April; accepted 20 August 2012.**

**Published online 14 October 2012.**

- Björklund, A. & Dunnett, S. B. Dopamine neuron systems in the brain: an update. *Trends Neurosci.* **30**, 194–202 (2007).
- Bromberg-Martin, E. S., Matsumoto, M. & Hikosaka, O. Dopamine in motivational control: rewarding, aversive, and alerting. *Neuron* **68**, 815–834 (2010).
- Schultz, W. Multiple dopamine functions at different time courses. *Annu. Rev. Neurosci.* **30**, 259–288 (2007).
- Lammel, S. *et al.* Unique properties of mesoprefrontal neurons within a dual mesocorticolimbic dopamine system. *Neuron* **57**, 760–773 (2008).
- Lammel, S., Ito, D. I., Roeper, J. & Malenka, R. C. Projection-specific modulation of dopamine neuron synapses by aversive and rewarding stimuli. *Neuron* **70**, 855–862 (2011).
- Margolis, E. B., Mitchell, J. M., Ishikawa, J., Hjelmstad, G. O. & Fields, H. L. Midbrain dopamine neurons: projection target determines action potential duration and dopamine D(2) receptor inhibition. *J. Neurosci.* **28**, 8908–8913 (2008).
- Sesack, S. R. & Grace, A. A. Cortico-basal ganglia reward network: microcircuitry. *Neuropsychopharmacology* **35**, 27–47 (2010).
- Geisler, S., Derst, C., Veh, R. W. & Zahm, D. S. Glutamatergic afferents of the ventral tegmental area in the rat. *J. Neurosci.* **27**, 5730–5743 (2007).
- Berridge, K. C., Robinson, T. E. & Aldridge, J. W. Dissecting components of reward: 'liking', 'wanting', and learning. *Curr. Opin. Pharmacol.* **9**, 65–73 (2009).
- Cohen, J. Y., Haesler, S., Vogt, L., Lowell, B. B. & Uchida, N. Neuron-type-specific signals for reward and punishment in the ventral tegmental area. *Nature* **482**, 85–88 (2012).
- Guarraci, F. A. & Kapp, B. S. An electrophysiological characterization of ventral tegmental area dopaminergic neurons during differential pavlovian fear conditioning in the awake rabbit. *Behav. Brain Res.* **99**, 169–179 (1999).
- Kim, Y., Wood, J. & Moghaddam, B. Coordinated activity of ventral tegmental neurons adapts to appetitive and aversive learning. *PLoS ONE* **7**, e29766 (2012).
- Tan, K. R. *et al.* GABA neurons of the VTA drive conditioned place aversion. *Neuron* **73**, 1173–1183 (2012).
- Matsumoto, M. & Hikosaka, O. Two types of dopamine neuron distinctly convey positive and negative motivational signals. *Nature* **459**, 837–841 (2009).
- van Zessen, R., Phillips, J. L., Budygin, E. A. & Stuber, G. D. Activation of VTA GABA neurons disrupts reward consumption. *Neuron* **73**, 1184–1194 (2012).
- Wickersham, I. R., Finke, S., Conzelmann, K. K. & Callaway, E. M. Retrograde neuronal tracing with a deletion-mutant rabies virus. *Nature Methods* **4**, 47–49 (2007).
- Watabe-Uchida, M., Zhu, L., Ogawa, S. K., Vamanrao, A. & Uchida, N. Whole-brain mapping of direct inputs to midbrain dopamine neurons. *Neuron* **74**, 858–873 (2012).
- Hikosaka, O. The habenula: from stress evasion to value-based decision-making. *Nature Rev. Neurosci.* **11**, 503–513 (2010).
- Forster, G. L. & Blaha, C. D. Laterodorsal tegmental stimulation elicits dopamine efflux in the rat nucleus accumbens by activation of acetylcholine and glutamate receptors in the ventral tegmental area. *Eur. J. Neurosci.* **12**, 3596–3604 (2000).
- Lodge, D. J. & Grace, A. A. The laterodorsal tegmentum is essential for burst firing of ventral tegmental area dopamine neurons. *Proc. Natl Acad. Sci. USA* **103**, 5167–5172 (2006).
- Hou, T. C., Geisler, S., Marinelli, M., Degarmo, B. A. & Zahm, D. S. The mesopontine rostromedial tegmental nucleus: a structure targeted by the lateral habenula that projects to the ventral tegmental area of Tsai and substantia nigra compacta. *J. Comp. Neurol.* **513**, 566–596 (2009).
- Kaufling, J., Veinante, P., Pawlowski, S. A., Freund-Mercier, M. J. & Barrot, M. Afferents to the GABAergic tail of the ventral tegmental area in the rat. *J. Comp. Neurol.* **513**, 597–621 (2009).
- Christoph, G. R., Leonzio, R. J. & Wilcox, K. S. Stimulation of the lateral habenula inhibits dopamine-containing neurons in the substantia nigra and ventral tegmental area of the rat. *J. Neurosci.* **6**, 613–619 (1986).
- Hou, T. C., Fields, H. L., Baxter, M. G., Saper, C. B. & Holland, P. C. The rostromedial tegmental nucleus (RMTg), a GABAergic afferent to midbrain dopamine neurons, encodes aversive stimuli and inhibits motor responses. *Neuron* **61**, 786–800 (2009).
- Ji, H. & Shepard, P. D. Lateral habenula stimulation inhibits rat midbrain dopamine neurons through a GABA(A) receptor-mediated mechanism. *J. Neurosci.* **27**, 6923–6930 (2007).
- Omelenko, N., Bell, R. & Sesack, S. R. Lateral habenula projections to dopamine and GABA neurons in the rat ventral tegmental area. *Eur. J. Neurosci.* **30**, 1239–1250 (2009).
- Araki, M., McGeer, P. L. & Kimura, H. The efferent projections of the rat lateral habenular nucleus revealed by the PHA-L anterograde tracing method. *Brain Res.* **441**, 319–330 (1988).
- Cornwall, J., Cooper, J. D. & Phillipson, O. T. Afferent and efferent connections of the laterodorsal tegmental nucleus in the rat. *Brain Res. Bull.* **25**, 271–284 (1990).
- Vertes, R. P., Fortin, W. J. & Crane, A. M. Projections of the median raphe nucleus in the rat. *J. Comp. Neurol.* **407**, 555–582 (1999).
- Sanchez, C. J., Bailie, T. M., Wu, W. R., Li, N. & Sorg, B. A. Manipulation of dopamine d1-like receptor activation in the rat medial prefrontal cortex alters stress- and cocaine-induced reinstatement of conditioned place preference behavior. *Neuroscience* **119**, 497–505 (2003).
- Tsai, H. C. *et al.* Phasic firing in dopaminergic neurons is sufficient for behavioral conditioning. *Science* **324**, 1080–1084 (2009).
- Witten, I. B. *et al.* Recombinase-driver rat lines: tools, techniques, and optogenetic application to dopamine-mediated reinforcement. *Neuron* **72**, 721–733 (2011).
- Robbins, T. W. & Arnsten, A. F. The neuropsychopharmacology of fronto-executive function: monoaminergic modulation. *Annu. Rev. Neurosci.* **32**, 267–287 (2009).
- Lecourtier, L., DeFrancesco, A. & Moghaddam, B. Differential tonic influence of lateral habenula on prefrontal cortex and nucleus accumbens dopamine release. *Eur. J. Neurosci.* **27**, 1755–1762 (2008).
- Li, B. *et al.* Synaptic potentiation onto habenula neurons in the learned helplessness model of depression. *Nature* **470**, 535–539 (2011).
- Lecourtier, L. & Kelly, P. H. Bilateral lesions of the habenula induce attentional disturbances in rats. *Neuropsychopharmacology* **30**, 484–496 (2005).
- Shepard, P. D., Holcomb, H. H. & Gold, J. M. Schizophrenia in translation: the presence of absence: habenular regulation of dopamine neurons and the encoding of negative outcomes. *Schizophr. Bull.* **32**, 417–421 (2006).
- Stamatakis, A. M. & Stuber, G. D. Activation of lateral habenula inputs to the ventral midbrain promotes behavioural avoidance. *Nature Neurosci.* **15**, 1105–1107 (2012).

**Supplementary Information** is available in the online version of the paper.

**Acknowledgements** We thank the Stanford Neuroscience Imaging Core, the Stanford Neuroscience Behavior Phenotyping and Pharmacology Core and the Stanford Neuroscience Gene Vector and Virus Core (all supported by National Institutes of Health grant NIH NS069375). This work was supported by grants from the Simons Foundation and NIH (to R.C.M.). K.D. is supported by the NIH, the DARPA REPAIR program, and the Wieggers Family Fund. S.L. is supported by a fellowship from the German Academy of Sciences Leopoldina. B.K.L. is supported by a Davis Foundation Postdoctoral Fellowship in Eating Disorders Research. K.M.T. is supported by the JPB Foundation and NIMH.

**Author Contributions** S.L., B.K.L. and R.C.M. designed the study, interpreted results and wrote the paper. S.L. and B.K.L. performed stereotaxic injections, optogenetic experiments and electrophysiology. S.L., C.R., M.J.B. and K.W.H. performed immunohistochemistry. B.K.L. and K.W.H. generated viruses. K.T. and K.D. provided optogenetics training and resources. All authors edited the paper.

**Author Information** Reprints and permissions information is available at [www.nature.com/reprints](http://www.nature.com/reprints). The authors declare no competing financial interests. Readers are welcome to comment on the online version of the paper. Correspondence and requests for materials should be addressed to R.C.M. ([malenka@stanford.edu](mailto:malenka@stanford.edu)).



## METHODS

**Animals.** Male adult (10–12 weeks of age) C57BL/6 (Charles River) or TH-Cre (B6.Cg-Tg(Th-cre)1Tmd/J; Jackson Laboratory) mice were used for all experiments. All procedures complied with the animal care standards set forth by the National Institutes of Health and were approved by Stanford University's Administrative Panel on Laboratory Animal Care.

**Virus generation.** The AAVs used in this study were generated as previously described<sup>39</sup> either by the Deisseroth laboratory (AAV-ChR2) or the Stanford Neuroscience Gene Vector and Virus Core (AAV-DIO-RVG). Rabies virus was generated from a full-length complementary DNA plasmid containing all components of the virus (SAD L16; a gift from K.-K. Conzelmann<sup>40</sup>). We replaced the RVG with eGFP, tdTomato or ChR2(H134R) fused to eYFP to generate virus expressing eGFP (RV-eGFP), tdTomato (RV-tdTomato) or ChR2(H134R) (RV-ChR2). To collect the virus from this cDNA we used a modified version of published protocols<sup>40,41</sup>. In brief, HEK293T cells were transfected with a total of six plasmids; four expressing the viral components pTIT-N, pTIT-P, pTIT-G and pTIT-L; one plasmid expressing T7 RNA polymerase (pCAGGS-T7), and the aforementioned glycoprotein-deleted viral cDNA plasmid expressing eGFP, tdTomato or ChR2. For the amplification of the virus, the media bathing these HEK293T cells was collected 3–4 days after transfection and moved to baby hamster kidney cells stably expressing viral glycoprotein (BHK-B19G)<sup>41</sup>. After 3 days, the media from BHK-B19G cells was collected, centrifuged for 5 min at 3,000g to remove cell debris, and concentrated by ultracentrifugation (55,000g for 2 h). Pellets were suspended in DPBS, aliquoted and stored at  $-80^{\circ}\text{C}$ . The titre of concentrated virus was measured by infecting HEK293 cells and monitoring fluorescence. Plasmids expressing the viral components were gifts from K.-K. Conzelmann and I. Wickersham. BHK cells stably expressing B19G were a gift from E. Callaway.

**Stereotaxic injections and optic fibre/cannula implantations.** As previously described<sup>4,5</sup>, all stereotaxic injections were performed under general ketamine-medetomidine anaesthesia and using a stereotaxic instrument (Kopf Instruments). Adult (10–12 weeks; 25–30 g) male C57BL/6 and TH-Cre mice were group-housed until surgery. Mice were maintained on a 12:12 light cycle (lights on at 07:00). For retrobead labelling (100 nl; LumaFluor Inc.) mice were injected unilaterally with fluorescent retrobeads in the NAc lateral shell (bregma, 1.45 mm; lateral, 1.75 mm; ventral, 4.0 mm), NAc medial shell (bregma, 1.78 mm; lateral, 0.5 mm; ventral, 4.1 mm), or mPFC (two injections at four different sites: bregma, 1.95 mm, 2.05 mm, 2.15 mm and 2.25 mm; lateral, 0.27 mm; ventral, 2.1 mm and 1.6 mm; injected total volume in mPFC, 400 nl; the target area was the prelimbic and infralimbic cortex) using a 1  $\mu\text{l}$  Hamilton syringe (Hamilton). Note that these empirically derived stereotaxic coordinates do not precisely match those given in the mouse brain atlas<sup>42</sup>, which we used as references for the injection-site images. On average, the caudo-rostral axis appeared to be approximately shifted caudally by 400  $\mu\text{m}$ . Little labelling was observed in the pipette tract (that is, cingulate and motor cortices for mPFC injections or in the dorsal striatum for NAc lateral shell injections). To allow adequate time for retrograde transport of the retrobeads into the somas of midbrain dopamine neurons, minimal survival periods before sacrifice depended on the respective injection areas: NAc lateral shell, 3 days; NAc medial shell, 14 days; mPFC, 21 days. For viral infections a small amount of concentrated virus solution (0.5–1  $\mu\text{l}$  RV-eGFP, RV-tdTomato or RV-ChR2) or AAV-DIO-RVG or AAV-ChR2 was injected unilaterally in the LDT (bregma,  $-5.0$  mm; lateral, 0.5 mm; ventral, 3.0 mm) or LHb (bregma,  $-1.58$  mm; lateral, 0.4 mm; ventral, 2.65 mm) or into the VTA (bregma,  $-3.4$  mm; lateral, 0.35 mm; ventral, 4.0 mm) or mPFC or NAc lateral shell (same coordinates as for retrobead injections) using a syringe pump (Harvard Apparatus) at a slow rate (100–150 nl  $\text{min}^{-1}$ ). The injection needle was withdrawn 5 min after the end of the infusion.

For the dual virus injections (Supplementary Fig. 11), one virus (RV-eGFP or RV-tdTomato) was injected into the VTA and the other was injected into either the ventral pallidum (bregma, 0.62 mm; lateral, 1.10 mm; ventral, 4.75 mm), lateral septum (bregma, 0.62 mm; lateral, 0.35 mm; ventral, 3.0 mm), lateral hypothalamus (bregma,  $-0.94$  mm; lateral, 1.00 mm; ventral, 4.75 mm), mPFC (two injections at four different sites: bregma, 1.95 mm, 2.05 mm, 2.15 mm and 2.25 mm; lateral, 0.27 mm; ventral, 2.1 mm and 1.6 mm), mediodorsal thalamic nucleus (bregma,  $-1.22$  mm; lateral, 0.25 mm; ventral, 3.25 mm) or supraoculomotor central grey (bregma,  $-4.04$  mm; lateral, 0.3 mm; ventral, 2.7 mm). For anterograde labelling of LDT and LHb terminals in the VTA the anterograde tracer PHA-L (50 nl; 2.5% in 0.01 M phosphate buffer; Vector) was injected into the LDT or LHb (same coordinates as for virus injections). The survival period for the PHA-L-injected animals was 3 weeks and for the AAV-ChR2 injected animals 8–12 weeks.

For behavioural experiments, mice that were injected with RV-eGFP or RV-ChR2 in the VTA received unilateral implantation of a doric patch-cord chronically implantable fibre (NA = 0.22; Doric lenses) over the LDT (bregma,  $-5.0$  mm, lateral, 0.5 mm, ventral, 2.0 mm) or LHb (bregma,  $-1.58$  mm, lateral, 0.4 mm, ventral, 2.0 mm). One layer of adhesive cement (C&B metabond; Parkell) followed

by cranioplastic cement (Dental cement) was used to secure the fibre guide system to the skull. The incision was closed with a suture and tissue adhesive (Vetbond; Fisher). The animal was kept on a heating pad until it recovered from anaesthesia. For intra-VTA stimulation of LHb or LDT axon terminals, AAV-ChR2 was injected into LHb or LDT, respectively. Ten weeks after the virus injection a doric optic fibre was implanted unilaterally over the caudal medial VTA for stimulation of LHb axon terminals (bregma,  $-3.4$  mm; lateral, 0.35 mm; ventral, 3.6 mm) and over the lateral VTA for stimulation of LDT axon terminals (bregma,  $-3.4$  mm; lateral, 0.5 mm; ventral, 3.6 mm). Behavioural experiments were performed 2 weeks after the implantation. For microinjection of dopamine receptor antagonists into the mPFC or NAc lateral shell a guide cannula (PlasticOne) was implanted directly over the ipsilateral mPFC (bregma, 2.2 mm; lateral, 0.3 mm; ventral,  $-2.0$  mm) or NAc lateral shell (bregma, 1.45 mm; lateral, 1.75 mm; ventral, 4.0 mm) of the mice in which RV ChR2 injection into the VTA and the implantation of doric optic fibres were made. Optical fibre and cannula placements were confirmed in all animals. Although placements varied slightly from mouse to mouse, behavioural data from all mice were included in the study.

**Electrophysiology.** Mice were deeply anaesthetized with pentobarbital (200 mg  $\text{kg}^{-1}$  intraperitoneally; Ovation Pharmaceuticals). Coronal midbrain slices (250  $\mu\text{m}$ ) were prepared after intracardial perfusion with ice-cold artificial cerebrospinal fluid (ACSF) containing elevated (in mM): 50 sucrose, 125 NaCl, 25  $\text{NaHCO}_3$ , 2.5 KCl, 1.25  $\text{NaH}_2\text{PO}_4$ , 0.1  $\text{CaCl}_2$ , 4.9  $\text{MgCl}_2$  and 2.5 glucose (oxygenated with 95%  $\text{O}_2$  and 5%  $\text{CO}_2$ ). After 90 min of recovery, slices were transferred to a recording chamber and perfused continuously at 2–4 ml  $\text{min}^{-1}$  with oxygenated ACSF (125 NaCl, 25  $\text{NaHCO}_3$ , 2.5 KCl, 1.25  $\text{NaH}_2\text{PO}_4$ , 11 glucose, 1.3  $\text{MgCl}_2$  and 2.5  $\text{CaCl}_2$ ) at  $\sim 30^{\circ}\text{C}$ . For the recording of EPSCs, picrotoxin (50  $\mu\text{M}$ ; Sigma) was added to block inhibitory currents mediated by GABA<sub>A</sub> receptors. The internal solution contained (in mM): 117 CsCH<sub>3</sub>SO<sub>3</sub>, 20 HEPES, 0.4 EGTA, 2.8 NaCl, 5 TEA, 4 MgATP, 0.3 NaGTP, 5 QX314, 0.1 spermine, and 0.1% neurobiotin. For recording of IPSCs the internal solution contained (in mM): 130 CsCl, 1 EGTA, 10 HEPES, 2 MgATP, 0.2 NaGTP and 0.1% neurobiotin (for both internal solutions pH 7.35, 270–285 mOsm). Patch pipettes (3.8–4.4 M $\Omega$ ) were pulled from borosilicate glass (G150TF-4; Warner Instruments).

Labelled dopamine neurons were visualized with a 40X water-immersion objective on an upright fluorescent microscope (BX51WI; Olympus) equipped with infrared-differential interference contrast video microscopy and epifluorescence (Olympus) for detection of retrobeads. ChR2 was stimulated by flashing 473 nm light (5-ms pulses; 0.1 Hz; 1–2 mW) through the light path of the microscope using a ultrahigh-powered light-emitting diode (LED) powered by an LED driver (Prizmatix, Modiin Ilite) under computer control. The light intensity of the LED was not changed during the experiments and the whole slice was illuminated. A dual lamp house adaptor (Olympus) was used to switch between fluorescence lamp and LED light source. EPSCs were recorded in whole-cell voltage clamp (Multiclamp 700B, Molecular Devices), filtered at 2 kHz, digitized at 10 kHz (ITC-18 interface, HEKA) and collected online using custom IgorPro software (Wavemetrics). Series resistance (15–25 M $\Omega$ ) and input resistance were monitored online with a 4-mV hyperpolarizing step (50 ms) given with each afferent stimulus. VTA/substantia nigra and RMTg neurons were voltage-clamped at  $-70$  mV and EPSC or IPSC amplitudes were calculated by measuring the peak current from the average EPSC or IPSC response from 10–15 consecutive sweeps.

For pharmacological characterization light-evoked EPSCs or IPSCs were recorded for 5 min followed by bath perfusion of 10  $\mu\text{M}$  CNQX (Tocris Bioscience) or 50  $\mu\text{M}$  picrotoxin (Sigma) for an additional 10 min, respectively. 10–15 consecutive sweeps pre- and post-drug were averaged and peak EPSCs or IPSCs amplitudes were then measured. For detection of IPSCs, labelled cells were recorded from the caudal VTA in slices that contained the RMTg. For determination of dopamine or GABAergic phenotype, neurons were filled with neurobiotin (Vector) during the patch clamp experiment, then fixed in 4% paraformaldehyde (PFA) and 24 h later immunostained for TH or GAD67. Approximately 80% of all whole-cell patch clamped neurons could be successfully recovered. The dopamine phenotype or GABAergic phenotype (in the RMTg) was confirmed in all of these neurons.

**Immunohistochemistry.** Immunohistochemistry and confocal microscopy were performed as described previously in refs 4 and 5. In brief, after intracardial perfusion with 4% paraformaldehyde in PBS, pH 7.4, the brains were post-fixed overnight and coronal midbrain slices (50 or 100  $\mu\text{m}$ ) were prepared. The primary antibodies used were mouse anti-TH (1:1,000; Millipore), rabbit anti-TH (1:1,000; Calbiochem), rabbit anti-PHA-L (1:1,000; Vector), goat anti-EAAC1 (1:1,000; Millipore), rabbit anti-Chat (1:200; Millipore), mouse anti-GAD67 (clone 1G10.2; 1:500; Millipore), rabbit anti-FOS (1:500, Calbiochem) and rabbit anti-NeuN (neuronal nuclei; 1:1,000; Millipore). The secondary antibodies used were Alexa Fluor 488 anti-rabbit, Alexa Fluor 546 anti-goat, Alexa Fluor 546 anti-rabbit, Alexa Fluor 546 anti-mouse, Alexa Fluor 647 anti-rabbit, Alexa Fluor 647 anti-mouse (all 1:750), Alexa Fluor 488 streptavidin (1:1,000) (all Molecular

Probes). Image acquisition was performed with a confocal system (Zeiss LSM510) using 10X, 40X or 63X objectives and on a Zeiss AxioImager M1 upright wide-field fluorescence/differential interference contrast microscope with charged-coupled device camera using 2.5X and 10X objectives. Images were analysed using the Zeiss LSM Image Browser<sup>39</sup> software and ImageJ software.

For quantification of ChR2-eYFP fluorescence intensity and quantification of FOS-positive cells, confocal images were acquired using identical pinhole, gain and laser settings. Images in the medial and lateral VTA as well as the substantia nigra from the same tissue sections were acquired at the same focus level. The medial and lateral VTA was defined as the area that corresponds to the anatomical location of distinct dopamine subpopulations<sup>4,5</sup>. The medial VTA was defined as the region comprising the medial paraventricular nucleus and medial parabrachial pigmented nucleus, whereas the lateral VTA was defined as the lateral parabrachial pigmented nucleus (Supplementary Fig. 8c). No additional post-processing was performed on any of the collected images. ChR2 fluorescence intensity was then quantified using a scale from 0 to 255 in ImageJ to determine the mean intensity across the entire image. For retrobeads, AAV and PHA-L injections and viral injections in the mPFC and NAc lateral shell, the injection sites were confirmed in all animals by preparing coronal sections (100 µm). Counterstaining of injection sites was performed with green or red Nissl (NeuroTrace 500/525 or 530/615, Molecular Probes).

We routinely carried out complete serial analyses of the injection sites. Animals with notable contaminations outside target areas were discarded (see ref. 4 for serial analysis of retrobead injection sites and definition of dopamine target areas). For viral injections into the VTA we confirmed that all animals had the centre of the viral injection located in the caudal VTA (Bregma, -3.4 mm). However, quantification of the 'spread' of the RV-ChR2 injected into the VTA is difficult because for expression of the transgene, the rabies virus must be taken up by terminals and the transgene must be synthesized in the cytosol and then transported within the axons. Any eYFP within the VTA and adjacent structures will represent axons/terminals of cells that project to the VTA and adjacent structures as well as the cell bodies of neurons (that is, RMTg) that have local connectivity within the VTA and adjacent structures. Thus transgene expression in structures adjacent to the VTA does not indicate that Lhb or LDT neurons project to these structures. Nevertheless, in Supplementary Fig. 15 we present a serial reconstruction for the caudo-rostral extent of the midbrain showing the expression of ChR2-eYFP 1 week after injection of RV-ChR2 into the VTA ( $n = 5$  mice). TH-stained coronal mid-brain sections (100 µm) were prepared from the injected mice and reconstructed using NeuroLucida software (MicroBrightField). Sections were labelled relative to bregma using landmarks and neuroanatomical nomenclature as described in ref. 42. We report all brain areas in which detectable eYFP was observed. The strongest transgene expression was observed in the caudal VTA and several of its distinct subnuclei, most commonly in the IPN. We also always detected high transgene expression in the RMTg. Thus when referred to in the text, the VTA includes the RMTg, which was originally termed the 'tail of the VTA'<sup>22</sup>.

Because the IPN expressed ChR2-eYFP after intra-VTA injections, we conducted additional double retrograde tracing experiments in which we injected small amounts of green retrobeads (20 nl; LumaFluor Inc.) into the IPN (bregma, -3.9 mm; lateral, 0 mm; ventral, 4.55 mm) and red Retrobeads (60 nl; LumaFluor Inc.) into the VTA (bregma, -3.4 mm; lateral, 0.35 mm; ventral, 4.0 mm). Fluorescently labelled latex retrobeads were used in these experiments ( $n = 2$  mice) because they show very limited diffusion from the injection site even after several weeks *in vivo*, and thus can be highly localized. Although a large number of cells in the Lhb contained red beads (~84%, 79 out of 94 cells), confirming a projection from this structure to the VTA, only a small proportion of these cells (~12%, 11 out of 94 cells) also contained green beads (Supplementary Fig. 16). By contrast, a large number of medial habenula cells contained green beads (~98%, 214 out of 218 cells) and less than 2% (3 out of 218 cells) of these also contained red beads (Supplementary Fig. 16), demonstrating that the medial habenula preferentially projects to the IPN. In the LDT, many cells (>100) contained red beads and none of these cells contained green beads (Supplementary Fig. 16). These results indicate that LDT cells likely only project to VTA and not the IPN, whereas the proportion of Lhb neurons that project to the IPN in addition to the VTA is small.

For quantification of the expression of RV-ChR2 in the LDT and Lhb 50 µm coronal sections from mice which had been injected with RV-ChR2 in the VTA were stained for NeuN. In total, 66 confocal images from the LDT and 55 confocal images from the Lhb were obtained using a 40X objective ( $n = 3$  mice). The percentage of ChR2-eYFP-positive cells relative to the number of NeuN-positive cells in a 125 µm × 125 µm area was analysed using the ImageJ software. Approximately 20% of all NeuN-positive LDT and Lhb neurons expressed ChR2-eYFP after RV-ChR2 injection into the VTA (Supplementary Fig. 15).

**Behavioural assays.** All behavioural tests were conducted during the same circadian period (13:00–19:00). The CPP and CPA protocols were performed in a rectangular cage with a left chamber measuring 28 cm × 24 cm with black and

white stripes on the walls and a metal grill floor, a centre chamber measuring 11.5 cm × 24 cm with white walls and a smooth plastic floor and a right chamber measuring 28 cm × 24 cm with black and white squares on the walls and a punched metal floor. The apparatus was designed so that mice did not have any consistent bias for a particular chamber (Supplementary Fig. 4b). The CPP and CPA tests consisted of 3 sessions over 3 days. On day 1 (1 week after infusion of RV-eGFP or RV-ChR2 into the VTA), individual mice were placed in the centre chamber and allowed to freely explore the entire apparatus for 15 min (pre-test). On day 2 mice were confined to one of the side chambers for 30 min during optical stimulation. Stimulation in left or right chambers was counterbalanced across mice. For stimulation the optical fibre was connected to a 473-nm laser diode (OEM Laser Systems) through an FC/PC adaptor. Laser output was controlled using a Master-8 pulse stimulator (A.M.P.I.), which delivered 8 pulses of 5-ms light flashes at 30 Hz every 5 s (phasic stimulation) or 5-ms light flashes delivered at 1 Hz (low-frequency stimulation). For stimulation of LDT and Lhb axon terminals in the VTA, 15 pulses of 5-ms light flashes at 30 Hz every 2 s were delivered. Light output through the optical fibres was adjusted to 20 mW using a digital power meter console (Thorlabs) and was checked before and after stimulation of each mouse. On day 3, similar to day 1, mice were placed in the centre chamber and allowed to freely explore the entire apparatus for 15 min (post-test 1). After post-test 1 the blue-light laser was switched on and the mouse received phasic or low-frequency stimulation for whenever it was in the chamber in which it had been conditioned on day 2 for a total duration of 15 min (post-test 2). There was no interruption between post-test 1 and post-test 2. A video tracking system (BIOBSERVE) recorded all animal movements. To calculate preference or aversion during post-test 1, we divided the relative time (in %) the mouse spent during post-test 1 in the conditioned chamber (that is, the chamber in which it received either phasic or low-frequency light stimulation of LDT or Lhb inputs to the VTA) by the relative time (in %) the mouse spent in this chamber during the pre-test (post-test 1/pre-test ratio). During post-test 2, preference or aversion was calculated by dividing the relative time (in %) the mouse spent during post-test 2 in the conditioned chamber by the relative time (in %) the mouse spent in this chamber during the pre-test (post-test 2/pre-test ratio).

For the microinjection of the D1 dopamine receptor antagonist SCH23390 into the mPFC and the microinjection of the D1 and D2 dopamine receptor antagonists SCH23390 and raclopride into the NAc lateral shell, a 33-gauge injector cannula connected to a syringe pump (Harvard Apparatus) was inserted into the guide cannula which had been implanted in the mPFC or NAc lateral shell. All micro-injections were delivered at a rate of 100 nl min<sup>-1</sup>. Injector cannulas remained in place for an additional minute before being removed. Drugs were infused 5 min before the beginning of the light stimulation on day 2. For the pharmacological control experiments, the animals were treated identically except no optical stimulation was provided. Doses of drugs used for microinjections were: 50 ng SCH23390 in 0.2 µl saline (mPFC); 300 ng SCH23390 and 3 µg raclopride in 0.3 µl saline/DMSO (NAc lateral shell).

The open-field test was conducted on different cohorts of mice to measure the effect of optogenetic stimulation on anxiety-like responses and general locomotor ability. The mice were placed in the chamber (50 × 50 cm) and their movement was recorded and analysed for 18 min using the same video-tracking software that was used in the CPP and CPA tests (BIOBSERVE). After 3 minutes without optical stimulation, phasic stimulation was turned on for three 3-min epochs interspersed with 3-min epochs of no stimulation. For all analyses and graphs where total 'off' and 'on' conditions are displayed, the three 'off' epochs were pooled and the three 'on' epochs were pooled. The inner zone of the open-field chamber was defined as the 23 × 23 cm central square area.

For quantification of FOS immunoreactivity, LDT and Lhb inputs to the VTA were stimulated for 30 min using the phasic light-stimulation protocol. During this time the mice remained in their home cage. The mice were perfused with 4% PFA 60 min after the *in vivo* light stimulation and 24 h later immunohistochemistry was performed.

**Statistics.** Student's *t*-tests, Mann-Whitney U-tests or one-way ANOVA tests were used to determine statistical differences using GraphPad prism 5 (Graphpad Software). Bonferroni post hoc analysis was applied, when necessary, to compare means. Statistical significance was set at \* $P < 0.05$ , \*\* $P < 0.01$ , \*\*\* $P < 0.001$ . All data values are presented as mean ± s.e.m.

39. Zhang, F. *et al.* Optogenetic interrogation of neural circuits: technology for probing mammalian brain structures. *Nature Protocols* **5**, 439–456 (2010).
40. Mebatsion, T., Konig, M. & Conzelmann, K. K. Budding of rabies virus particles in the absence of the spike glycoprotein. *Cell* **84**, 941–951 (1996).
41. Wickersham, I. R., Sullivan, H. A. & Seung, H. S. Production of glycoprotein-deleted rabies viruses for monosynaptic tracing and high-level gene expression in neurons. *Nature Protocols* **5**, 595–606 (2010).
42. Franklin, K. & Paxinos, G. *The Mouse Brain in Stereotaxic Coordinates* (Elsevier, 2001).



Copyright of Nature is the property of Nature Publishing Group and its content may not be copied or emailed to multiple sites or posted to a listserv without the copyright holder's express written permission. However, users may print, download, or email articles for individual use.